

Wall-Street: Smart Surface-Enabled 5G mmWave for Roadside Networking

Kun Woo Cho¹, Prasanthi Maddala², Ivan Seskar², Kyle Jamieson¹
Princeton University¹, Rutgers University²

Abstract

5G mmWave roadside networks promise high-speed wireless connectivity, but face significant challenges in maintaining reliable connections for users moving at high speed. Frequent handovers, complex beam alignment, and signal attenuation due to obstacles like car bodies lead to service interruptions and degraded performance. We present **Wall-Street**, a smart surface installed on vehicles to enhance 5G mmWave connectivity for users inside. Wall-Street improves mobility management by (1) steering outdoor mmWave signals into the vehicle, ensuring coverage for all users; (2) enabling simultaneous serving cell data transfer and candidate handover cell measurement, allowing seamless handovers without service interruption; and (3) combining beams from source and target cells during a handover to increase reliability. Through its flexible signal manipulation capabilities, Wall-Street provides uninterrupted high-speed connectivity for latency-sensitive applications in challenging mobile environments. We have implemented and integrated Wall-Street in the COSMOS testbed and evaluated its real-time performance with three gNBs and multiple mobile clients inside a surface-enabled vehicle, driving on a nearby road. In multi-UE scenarios, Wall-Street doubles the average TCP throughput and reduces delay by 30% over a baseline 5G Standalone handover protocol.

1 Introduction

Fifth Generation (5G) mobile wireless networks have recently introduced millimeter wave (mmWave) technology in the FR2 frequency band to meet the ever-increasing demand for high-speed, low-latency service [3]. With its abundant spectrum resources, mmWave communication has the potential to deliver multi-gigabit data rates, enabling a plethora of innovative applications such as virtual reality, augmented reality, and seamless streaming of ultra high-definition video [23]. However, the unique characteristics of mmWave signals pose significant challenges in maintaining reliable connectivity, particularly in high mobility scenarios [24].

One of the primary obstacles in mmWave communication is its susceptibility to blockage [17] and high path loss: due to its short wavelengths and limited diffraction capability, mmWave signals are easily obstructed by common obstacles such as buildings, foliage, and even the human body

[5, 13, 28, 33]. This necessitates a dense deployment of small cells to ensure adequate coverage, resulting in frequent handovers as users move between cells. Indeed, mmWave 5G New Radio (NR) experiences a handover (HO) significantly more often than LTE or low band 5G NR, [11, 20]. Moreover, the handover process in mmWave networks complicates the already-complex low band handover [7, 31], involving additionally precise alignment of the narrow beam between user equipment (UE) and base station (BS) [28], and requiring the UE to continuously measure the signal strength of neighboring cells and report it to the serving BS, which then decides when and to which cell to handover the UE.

High delays associated with mmWave handovers have significant impacts throughout the entire protocol stack, from the physical layer to the application layer, degrading quality of service (QoS) for end users, especially for latency-sensitive applications [11, 19]. To prepare a handover, the UE periodically suspends data communication with the serving BS to perform neighboring cell measurements. This process requires users to engage in an exhaustive search for the strongest signal from neighboring BSs, resulting in bufferbloat and slow growth of the congestion window [18]. Furthermore, the handover decision relies on these measurement reports, which may be outdated or lost due to the rapidly changing channel conditions and potential disconnections. This can trigger unnecessary handovers and lead to transport protocol connection timeouts, impacting overall network performance.

This paper presents the design and implementation of Wall-Street, a smart surface that transforms 5G mmWave connectivity, specifically for vehicular use scenarios. In such high-mobility scenarios, we install **Wall-Street** on vehicles to improve connectivity for users inside. Wall-Street leverages the concept of a programmable mmWave smart surface [6] to manipulate and steer mmWave signals, enabling seamless coverage and reliable communication for vehicle users. By strategically deploying Wall-Street on the exterior of vehicles, we aim to mitigate the impact of signal blockage and attenuation caused by the vehicle body, ensuring that mmWave signals can effectively penetrate and reach users inside the vehicle. Moreover, the handover (HO) process in mmWave networks consumes at least twice the energy

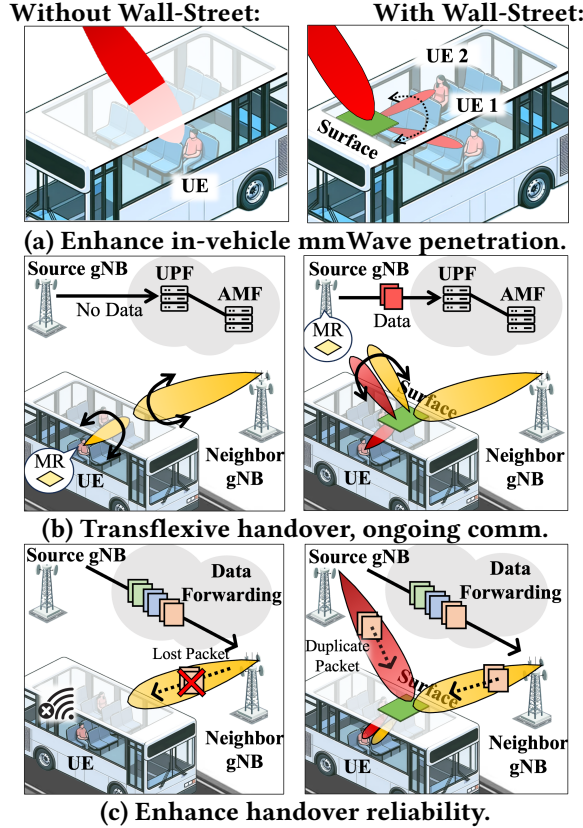


Figure 1— Wall-Street’s design innovations electronically split, shape, and steer mmWave transmissions in real time to enable seamless roadside 5G networks.

per unit distance, compared to low-band HOs [11]. Wall-Street reduces UE HO energy consumption by letting the surface perform neighboring cell signal strength measurements. Three key innovations of Wall-Street (Fig. 1) enable seamless vehicular-speed mmWave networking:

1. In-vehicle mmWave coverage. Wall-Street efficiently steers outdoor mmWave signals into a vehicle, providing consistent coverage for all users within (Fig. 1(a)) and eliminates the need for individual users to each undergo separate handover processes.

2. Seamless handover with concurrent communication. Innovating beyond previous programmable mmWave surfaces [6], Wall-Street is the first design that can simultaneously reflect, refract, and split the mmWave beam at arbitrary angles, with low signal strength loss. Leveraging this *transflexive* property, the Wall-Street system enables simultaneous data exchange and neighboring cell measurement by reflecting the synchronization signal bursts from neighboring cells directly to the serving BS while refracting the data communication link between the serving BS and UE, as shown in Fig. 1(b) (*right*). This innovative dual functionality

(simultaneous transmissive and reflective beam steering) allows for seamless handovers without service interruption, as the UE can continue to communicate with the serving base station (gNB) while the gNB performs the necessary measurements.

3. Make-before-break handover. At the moment of handover, when signal strength is typically weakest, Wall-Street facilitates the transmission of duplicate data packets from both the source and the new serving cell by combining two beams and steering them directly to the UE. This dual-beam combination significantly boosts the reliability during handover execution. By adjusting the power of the respective links, Wall-Street ensures an uninterrupted flow of data, minimizing packet loss and retransmissions.

We have designed and implemented Wall-Street hardware and integrated it into the COSMOS testbed [25], incorporating new PHY features on its USRP-based mmWave gNBs and UE. We mount Wall-Street on the rear door of an SUV vehicle and deploy multiple mobile UEs on the rear seat and back seat, with three gNBs placed on the first floor of a lab facing the road. We also implemented the 5G Standalone handover protocol and used it as a performance benchmark for our evaluation. To evaluate TCP end-to-end performance, we use a state-of-the-art mmWave ns-3 simulator [18] with our own modifications, in SA mode. The simulation is trace-driven, fed with PHY traces collected from real-time experiments. In multi-user scenarios, our results demonstrate a $2\times$ improvement in TCP throughput, a $0.7\times$ reduction in delay, and a $0.5\times$ reduction in unnecessary handover events compared to the baseline 5G Standalone handover protocol. Microbenchmarks investigate Wall-Street’s in-vehicle coverage improvement, beam tracking, and multi-link capabilities, and beam patterns, providing insights into new capabilities offered by Wall-Street.

2 Primer: 5G Mobility Management

We introduce the state of the art in 5G New Radio (NR) Standalone (SA) beam acquisition and tracking (§2.1), followed by 5G SA handover (§2.2), standardized in 3GPP 38.802 [1]. In contrast to Non-Standalone (NSA) handover, SA handover obviates the need to involve legacy 4G infrastructure in the handover [11], making it the cutting edge in 5G.

2.1 Initial Attachment and Tracking

Initial attachment of the UE to the gNB begins via a coarse spatial *beam sweep* of beam directions at both gNB and UE, which 3GPP calls *Procedure 1* (P-1). During the beam sweep in the first 5 ms of each period, the gNB transmits a *synchronization signal burst* comprised of 64 *Synchronization Signal Blocks* (SSBs). The gNB groups M SSBs together, transmitting all of them in the same direction before moving on

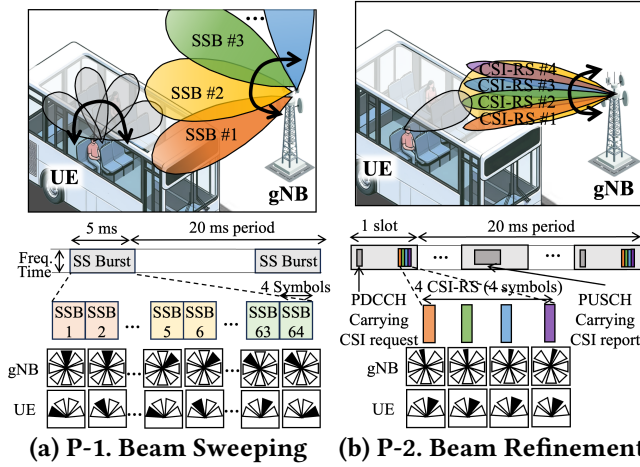


Figure 2— 5G SA beam acquisition and beam tracking.

to the next direction, as shown in Fig. 2(a). This transmission happens periodically, every 20 ms in the mmWave FR2 band by default. The UE scans all its receive directions in the corresponding time it takes the gNB to send M SSBs, so rendezvous is possible. The UE sends its measurement of the SSB's signal strength in a *measurement report* (MR) back the gNB, which confirms the transmit beam, thus initially aligning the transmit and receive beams. Finally, the UE and gNB exchange data through the selected beam patterns.

After initial attachment, the beam directions between the gNB and UE need to be refined in the face of UE mobility, a process 3GPP calls *Procedure 2* (P-2). The gNB uses transmit beams narrower than those used in P-1, and centered on the beam direction chosen during P-1. During P-2, the gNB scans different fine-grained directions on different channel state information reference signal (CSI-RS) resource blocks. The UE sends a CSI-RS to the gNB, which chooses the optimal fine-grained transmit beam direction. To track and refine UE beam directions, *Procedure 3* (P-3) uses CSI-RS combined with a static transmit beam and different UE receive beams.

2.2 5G SA Handover

Today's state of the art 5G SA handover is called *Xn handover*, named after the *Xn interface* that allows gNBs to exchange information related to the handover process. The handover procedure begins with the UE periodically generating and sending a MR containing the neighboring gNB's identifier, and the corresponding signal strength to the *source gNB* (with which the UE is currently communicating), which then takes the decision to start the handover procedure to the best *target gNB*. Finally, the target gNB completes the procedure. SA Xn handover is divided into three phases: *Preparation*, *Execution*, and *Completion*, as outlined in Fig. 3.

(1) Preparation phase. 5G SA relies on client-side feedback to trigger handovers. The source cell requests the UE to stop

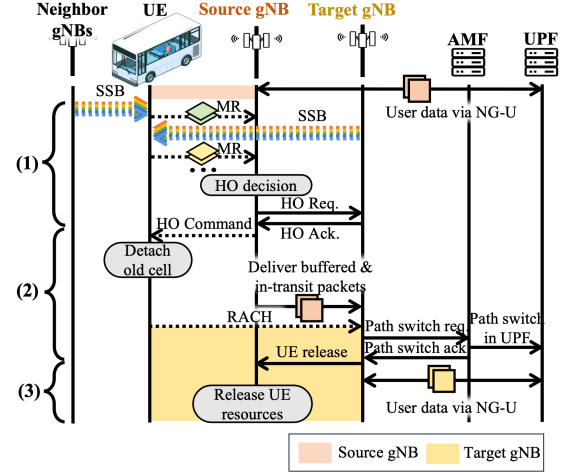


Figure 3— 5G SA Xn handover: (1) Preparation phase; (2) Execution phase; (3) Completion phase. Data exchange is denoted with orange and yellow rectangles.

the ongoing transmission and perform P-1 measurements to measure the received power of the reference signal (*Reference Signal Received Power*, or RSRP) for each neighboring cell. A common trigger for 5G handover is *event A3* [7, 31], which specifies that the signal strength of the neighboring cell is higher than that of the current serving cell by a certain hysteresis threshold, i.e.:

$$M_n - H > M_s \quad (1)$$

where M_n and M_s are the respective RSRPs of the neighboring and source cells, and H is a hysteresis parameter. To avoid ping-pong handover caused by signal fluctuations, a time-to-trigger (TTT) is used as the time hysteresis: the HO is triggered when Eq. (1) holds true for the TTT duration.

(2) Execution phase. The source gNB decides to initiate a handover and sends a *handover request* (HO Req) —Fig. 3, Step (2)—to the chosen target gNB over the Xn interface. The target BS responds with an ack, providing the necessary resources for the UE. Upon receiving the ack, the source BS sends a *Handover Command* (HO Command) to the UE, instructing it to detach from the source gNB and synchronize with the target gNB using the *Random Access Channel* (RACH) procedure. The source gNB forwards buffered and in-transit data to the target gNB.

(3) Completion phase. The target gNB sends a Path Switch request message to the the 5G Core (5GC), informing it about the handover and requesting a path update. The 5GC updates the path and sends an ack to the target gNB. The target gNB sends a UE Context Release message to the source gNB over the Xn interface, indicating that the handover is complete. The source gNB then releases the UE's context.

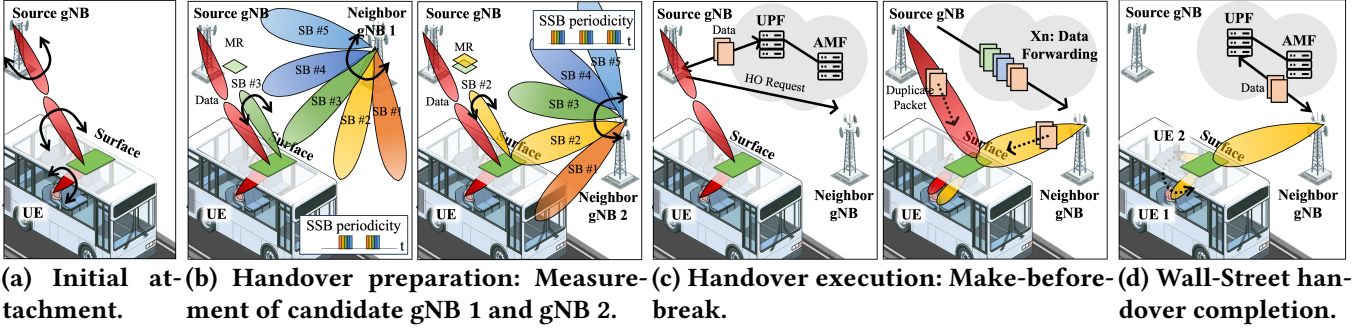


Figure 4— Wall-Street design overview: (a) Initial UE-RAN attachment (§3.2.1); (b) preparation using transfective surface power measurement to multiple cells (§3.3.1); (c) beam combining to enable make-before-break dual-cell connectivity (§3.3.2); (d) handover completion (§3.3.3).

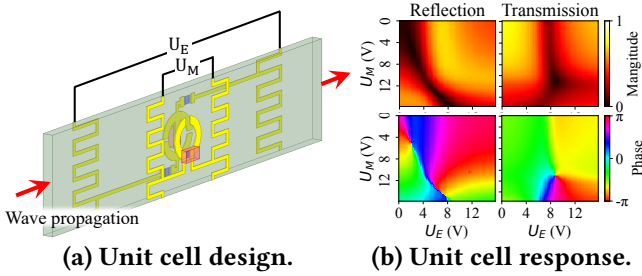


Figure 5— VNA measured unit cell response: reflection and transmission through the surface.

3 Design

This section presents the design of Wall-Street as shown in Fig. 4. Section 3.1 describes the Wall-Street surface. Section 3.2 explains the normal operations of UE attachment and tracking. Section 3.3 walks through Wall-Street’s handover.

3.1 Wall-Street Surface

The Huygens metasurface (HMS) is a metamaterial smart surface that reflects and refracts signals, and that prior work has demonstrated at 24 GHz [6]. Wall-Street for the first time demonstrates an HMS at 26 GHz. HMS comprises a layer of co-located orthogonal electric and magnetic dipoles, facing each other across dielectric substrate in a 3D structure, that introduces a discontinuity in the electromagnetic fields. It hence provides the means for manipulation of all attributes of the incident field, including its magnitude and phase, in both reflective and transmissive directions. Figure 5(a) shows Wall-Street’s electric unit cell on the back of the substrate and Wall-Street’s magnetic unit cell on the front of the substrate. Figure 5(b) presents Vector Network Analyzer (VNA) measurements of the unit cell response at 26 GHz. By adjusting the voltage applied to both the magnetic (U_M) and electric (U_E) unit cells, the surface achieves 2π phase coverage with near-unity magnitude for both reflection and transmission.

The Wall-Street surface is composed of 76 boards, each

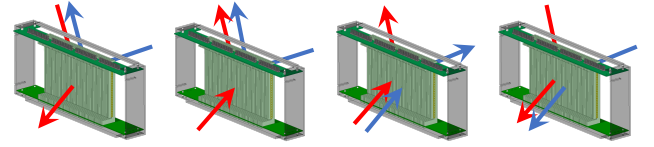


Figure 6— Wall-Street’s multi-beam operational modes (left to right): bi-directional split and combination for handover preparation and uni-directional split and combination for handover execution.

consisting of 28 co-located magnetic and electric unit cells. A control unit connected to Wall-Street supplies a set of voltages to the boards, and the beam is collectively shaped by all boards forming an array factor. Wall-Street has flexible multi-beam capabilities, including bi-directional splitting and combining and uni-directional splitting and combining, as shown in Fig. 6. Due to its angular reciprocity, the voltage configurations of splitting and combining are identical.

We refer the reader to Appendix A for the details on our design parameters. We will document and publicly release all PCB schematics, simulation scripts (HFSS and SPICE), and control codes.

3.2 Attachment and Tracking

Wall-Street’s normal operation requires UEs to attach to the RAN, and the RAN to track their movement. We detail how the UE initially attaches to the gNB and determines an optimal set of beam patterns via SSB measurements (§3.2.1), and how the gNB tracks the Wall-Street UE in motion (§3.2.2)

3.2.1 Initial Attachment. Similar to 5G NR, Wall-Street attachment adapt to function under practical timescales with a surface. First, a UE needs to be able to attach to the gNB of the RAN through Wall-Street. This process, shown at a high level in Fig. 4(a), begins with a SSB beam sweep at each of the gNB, Wall-Street, and UE, as detailed in Fig. 8(a). During a single SS burst, the UE fixes its beam angle while both Wall-Street and the gNB spatially sweep their beams. With

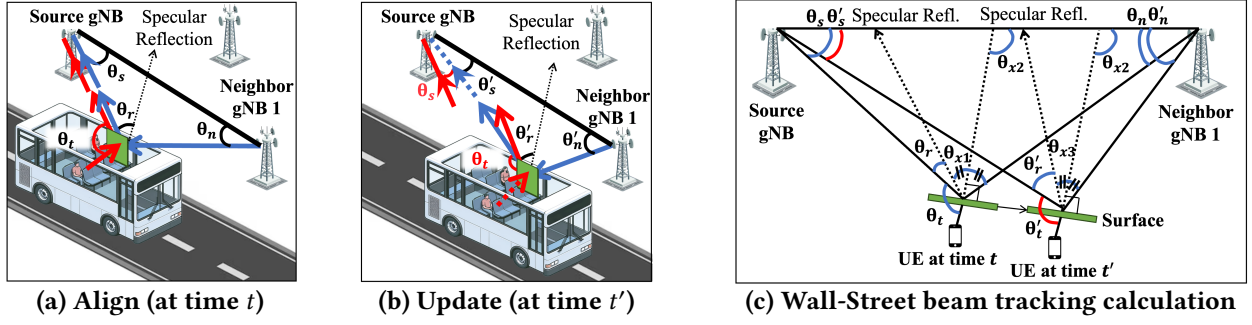


Figure 7— Beam tracking: surface-enabled beam tracking leverages neighboring gNBs to add path diversity.

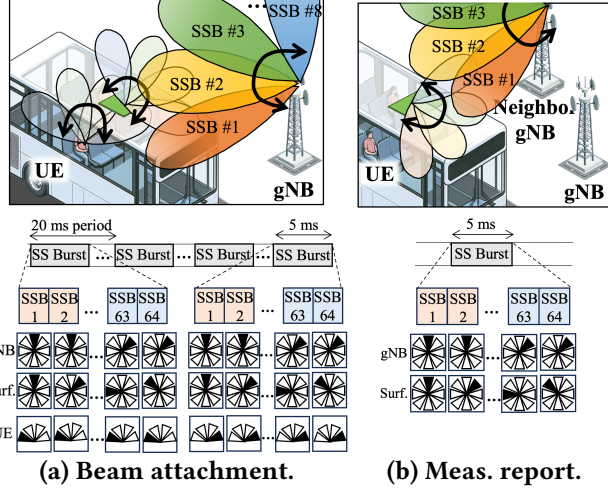


Figure 8— Wall-Street process: beam attachment and measurement report process. Beam attachment and measurement report require four SS bursts and one SS burst of five-millisecond duration.

each UE angle, the UE makes an SS Burst power measurement, each with a different beam pattern—each of which it feeds back to the gNB via a *beam report*. Practically, four SS bursts are needed (corresponding to each of four different UE receive beam patterns) for this initial paging search (80 ms).

Traditional repeaters require a $O(n^4)$ search for initial attachment, involving the gNB’s transmitting beam, repeater’s beam to gNB, repeater’s beam to UE, and UE’s receiving beam. This process takes about five seconds, which is impractical for rapidly moving vehicles. Our surface, however, directly manipulates the incident beam without separate receiving and transmitting modules, requiring a search in only one degree-of-freedom. This reduces initialization to a $O(n^3)$ search, considering only the gNB’s transmitting beam, surface’s beam to UE, and UE’s receiving beam. Moreover, Wall-Street’s angular reciprocity enables faster switching between uplink and downlink compared to repeaters.

3.2.2 Mobile User Tracking. Wall-Street adopts and leverages 3GPP P-2 and P-3 functionality for gNB- and UE-side

beam tracking, respectively (§2.1). In addition, Wall-Street devises the following surface-driven *path diversity tracking* algorithm that fuses measurement reports acquired from handover preparation, to bolster the reliability of the sensitive mmWave tracking process. Instead of relying on client-side report, the source gNB directly generates measurement reports by triggering Wall-Street to reflect neighboring gNB’s SSBs and receiving reflected SSBs, as shown in Fig. 4(b) and Fig. 8(b). We will further describe this procedure in §3.3.1.

After beam acquisition and measurement report at a given time t , the source gNB has knowledge of 1) θ_s , its own downlink beam angle, 2) θ_t , the angle by which Wall-Street deflects the UE’s uplink transmission, 3) θ_r , the (non-specular) angle¹ by which Wall-Street reflects a neighboring gNB’s downlink transmission, relative to the hypothetical specular reflection angle, because the source gNB has control over the surface, and 4) θ_n , the neighboring gNB’s downlink beam angle via mapping a SSB Beam ID from reflected SSBs, as diagrammed in Fig. 7(a). Importantly, we observe that every measurement report period of time (160 ms) a neighboring gNB sends an SSB burst, updating the source cell’s knowledge of parameters θ_r and θ_n (which we define θ'_r and θ'_n respectively), as shown in Fig. 7(b).

Now our objective is to calculate 1) $\Delta\theta_s$, a source gNB beam angle update, and 2) $\Delta\theta_t$, a surface transmissive beam steering angle update, both for the time step $t' - t$. For this, we first calculate the (hypothetical) specular reflection angle of the SS burst from the neighboring gNB 1 $\theta_{x1} = (180^\circ - (\theta_s + \theta_n) - \theta_r)/2$ as illustrated in Fig. 7(c). Then, we calculate the normal direction of the surface with respect to the source and neighbor gNBs $\theta_{x2} = \pi - (\theta_{n1} + \theta_{x1})$. In 160 ms, a vehicle moving at 40 mph travels less than three meters, so the surface orientation remains approximately the same. Hence we calculate the specular angle of SSB signals at t' as $\theta_{x3} = 180^\circ - \theta'_n + \theta_{x2}$. Finally, the source cell angle update is $\Delta\theta_s = \pi - (2\theta_{x3} + \theta_{r2}) - \theta_{n2} - \theta_{s1}$, and the surface transmissive beam deflection angle update is $\Delta\theta_t = (\theta_{x3} + \theta_{r2}) - (\theta_{x1} + \theta_{r1})$.

¹Specular reflection is a reflection at an equal but opposite angle to the incident light, as on mirrors.

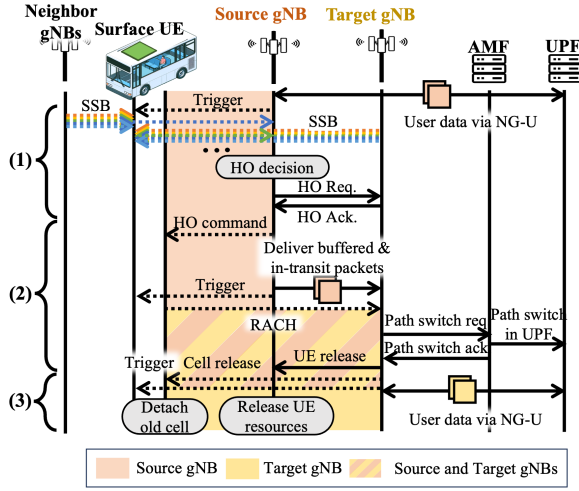


Figure 9— Wall-Street’s handover timeline: 1) Preparation, 2) Execution, and 3) Completion phases.

3.3 Cell-to-Cell Handover

This section describes Wall-Street’s cell to cell handover, the first step of which is preparation, which also leverages Wall-Street’s transreflective capability to take reflective measurements of neighboring cells while communication through the surface continues uninterrupted (§3.3.1). Section 3.3.2 presents our make-before-break handover, made possible by the combining of two beams: one from the source cell and another from the target cell. Section 3.3.3 concludes with a description of handover completion, releasing the source cell. Figure 9 summarizes the overall sequence of events.

3.3.1 Handover Preparation. We begin at the network layer, which is implemented inside the 5G core. Before handover, the source and neighbor gNB already have an active Xn (§2.2) connection, and the UE is in the RRC *connected* mode, sending and receiving data to and from the source gNB. Periodically, the source gNB sends a control signal via the robust, sub-6 GHz FR 1 band to Wall-Street, triggering the preparation at the physical layer that we describe next, a process that measures the RSRP of reflected SSBs. To avoid collisions, the gNBs separate their respective SSBs in frequency and time across different gNBs, allowing the source gNB to listen to other cells’ SSBs while simultaneously exchanging data with the UE.

Handover preparation at the PHY: Upon receiving a beam measurement trigger from the source gNB, Wall-Street alternates between bi-directional beam combination for uplink data (refracting signals from the UE and reflecting signals from neighboring gNBs) and bi-directional beam splitting for downlink data (refracting signals to the UE and reflecting signals from neighboring gNBs). During this process, the UE’s beam angle, the source gNB’s beam angle, and

Wall-Street’s refractive beam angle remain the same, and only Wall-Street’s reflective beam and the neighboring gNB’s beam sweep in one SS Burst, as depicted in Fig. 8(b).

As Wall-Street allows flexibility in the proportion of power allocated to its refractive and reflective beams on the uplink, now the issue arises of how to compute a power split. Given that the reflective beam travels a longer distance, it reduces the power allocated to the transmission link to the minimum required for maintaining communication, while directing the remaining power to the reflective link (see Fig. 22 in §5.3).

3.3.2 Handover Execution. The source gNB decides whether to initiate a handover using Eq. (1). To correctly trigger the HO event, the source gNB infers 3GPP-standard measurement report power readings based on Wall-Street’s reflective measurement report readings. We refer the reader to Appendix B for details. Upon proceeding, the source gNB sends a HO Req message to the target gNB. Upon receiving the corresponding HO ACK, the source gNB then triggers Wall-Street to switch to downlink beam combining and uplink beam splitting, and sends a HO command to the UE. Instead of detaching from the source gNB, however, the UE synchronizes with the target gNB via the RACH, using the 3GPP-standardized Dual Active Protocol Stack (DAPS) [2], maintaining two active protocol stacks. Upon receiving the HO command, the UE suspends the source cell *Signaling Radio Bearers* (SRBs), which are in charge of control-plane signaling (including Wall-Street control), and establishes SRBs for the target cell. The UE receives user data simultaneously from both source and target cells (on different channels), and we reconfigure the Packet Data Convergence Protocol (PDCP) layer to a common PDCP entity for the source and target user plane protocol stacks.

When the UE moves at vehicular speed, packets are prone to loss especially at the moment of handover when signal strength is typically weakest. So to ensure reliable packet delivery, the source and target gNBs send duplicate data packets during handover execution, and the UE’s PDCP layer reorders and de-duplicates them. For packet flow in the uplink, the UE sends the same packet to the source and target gNB, which forwards the received ACK through the Xn link and dequeues the packet in the shared buffer. Wall-Street’s PHY configuration remains the same for both downlink and uplink as in the preparation phase.

Handover execution at the PHY: Upon receiving a handover execution trigger from the serving gNB, Wall-Street switches between beam combining for the downlink packet flow from two gNBs and beam splitting for the uplink packet flow to two gNBs. Wall-Street simultaneously steers the downlink combination and uplink split at the same angle due to angular reciprocity. Specifically, given a certain biasing voltage configuration applied to the surface that creates a

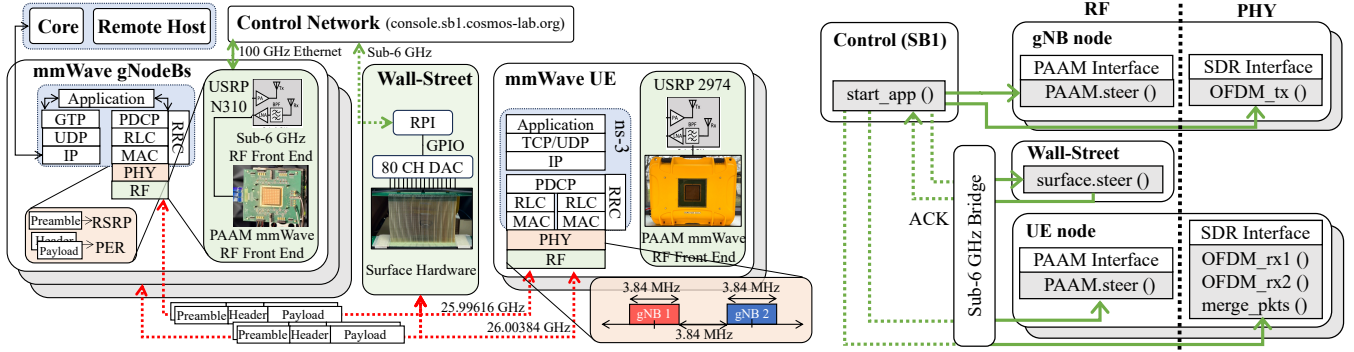


Figure 10— Wall-Street-COSMOS testbed integration: we integrate Wall-Street with COSMOS USRP-based gNBs and UE (left). We illustrate a simplified control flow of Wall-Street-integrated COSMOS testbed (right).

transmissive combination of two different angles for downlink signals, uplink signals impinging on the surface will be redirected toward the same angles in the uplink. Hence, angular reciprocity facilitates fast beam alignments as the surface configuration optimized for downlink transmissions works under the uplink communication, and vice versa.

During the make-before-break, the goal of the surface is to maintain simultaneous connections with both the source and target cells until the handover completes. Initially, power is equally divided between the two links. If either link fails, we increment its allocated gain to maintain the minimum required signal strength. If this gain increase is ineffective, we revert to the even power distribution.

3.3.3 Handover Completion. When Eq. (1) holds true for a threshold *time-to-handover* duration, the target cell completes the handover by sending the source cell a UE release indication and triggering a signal to Wall-Street indicate handover is complete. If handover fails, the UE immediately reverts to the source cell configuration and re-activates source cell SRBs for control-plane signaling. This prevents the UE from disconnecting completely.

Handover completion at the PHY: When the source gNB triggers a signal to complete handover, the surface maximizes the power of the transmission link with the new cell by reverting to a single beam mode. If the handover fails, instead maximizes the power of the link with the old cell, maintaining the connection for the UE. This approach eliminates the need to restart communication from the initial attachment phase if handover fails.

3.3.4 Multi-user Support. When a handover is executed for a UE in a vehicle, other UEs sharing the same Wall-Street within that vehicle do not need to undergo a separate handover procedure. Instead, the HO Request encapsulates the contexts of all UEs associated with each Wall-Street, allowing all UEs to be handed over simultaneously using the procedure above.

4 Implementation

We illustrate our Wall-Street implementation in Fig. 10. It consists of: (1) a surface hardware and control unit; (2) integration with the COSMOS testbed, implementing new PHY features; and (3) an ns-3 simulation for evaluating TCP end-to-end performance, using a state-of-the-art mmWave ns-3 simulator [18] with our own modifications. The simulation is trace-driven, fed with PHY traces collected from real-time experiments. The simulator implements a multi-user scenario as described in §3.3.4. In this setup, UE 2 does not undergo an independent handover procedure, but instead follows the handover decision made for UE 1.

4.1 Wall-Street Hardware

Two 40-channel AD5370 16-bit DACs provide independent control of the unit cells on each Wall-Street board, with each channel supplying a variable 0 to 16 V control voltage. To expedite the steering process, one channel supplies the voltage to two adjacent boards, enabling two DACs to independently control all boards, representing a savings of control logic relative to prior work [6]. The two DACs are each connected to the Serial Peripheral Interface (SPI) of a Raspberry Pi (RPI) through GPIO. The RPI listens for control signals from the COSMOS testbed control network, known as sandbox1 (SB1), via sub-6 GHz. Upon receiving a signal, it sends a command to the DACs, which then apply the appropriate voltage levels. These voltage levels are determined from a pre-stored voltage-to-phase look-up table. The steering speed of the Wall-Street hardware has been optimized to 0.2 ms for real-time implementation.

4.2 COSMOS Testbed

The COSMOS testbed comprises software-defined radios (USRPs) integrated with the IBM mmWave Phased-Array Antenna Module (PAAM) frontends (Fig. 10). The PAAM features 4 tiled RFICs, each with 32 TRx phase-shifting elements, supporting a total of 64 antennas. The PAAM offers

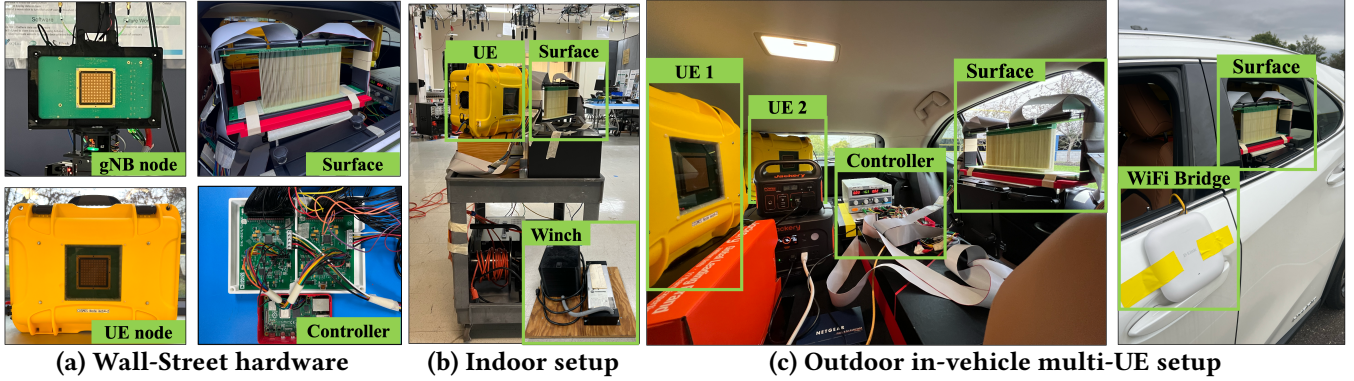


Figure 11— Wall-Street’s hardware implementation and testbed: showing (a) individual hardware components, (b) indoor experimental UE-side setup, and (c) outdoor in-vehicle UE-side configuration.

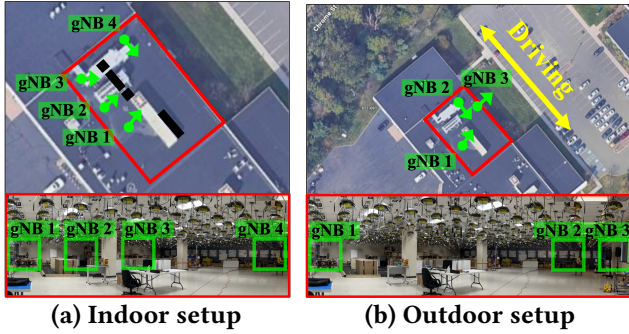


Figure 12— Experimental gNB-side testbed setup and map: we deploy gNBs on the first floor of a lab facing an outdoor parking lot. The vehicle is approximately 20 to 30 m from the gNBs. The arrow indicates the direction that each gNB node is facing at 0° , and each node sweeps the beam from -60° to 60° .

full access to beamforming control and latency as low as 10s of nanoseconds for low-latency MAC and hybrid beamforming. As shown in Fig. 11(a), our experimental setup employs two types of PAAM devices: two stationary PAAMs integrated with USRP N310s (maximum 65 dB gain) mounted on remotely controllable XY tables, and three portable PAAMs integrated with USRP 2974s (maximum 31 dB gain). For indoor scenarios, we utilize four gNBs: two stationary PAAMs (gNB 1 and 4) with a 35 dB gain and two portable PAAMs (gNB 2 and 3) with a 31 dB gain. In multi-UE outdoor scenarios, we use three gNBs: two stationary PAAMs (gNB 1 and 2) with a 65 dB gain and one portable PAAM (gNB 3) with a 31 dB gain, with the remaining portable PAAMs serving as UEs. The location of UEs remain the same with and without the surface. Since all nodes must be connected to the same control network (SB1), we use a Wi-Fi bridge operating at sub-6 GHz to send the control commands to outdoor UEs and the surface.

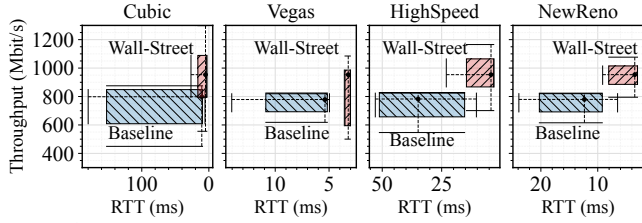
4.2.1 PHY implementation on COSMOS. We developed new features on the PHY layer of the COSMOS testbed, including OFDM packet transmission and reception at one or more channels, extraction of RSRP and Packet Error Rate (PER) from the packet, and IBM PAAM and Wall-Street beam control. Periodic bursts of OFDM packets are sent from two PAAMs in different frequency bands with 3.84 MHz separation, and the receiver simultaneously decodes packets from both transmitters by operating at a larger bandwidth. Specifically, the receiver extracts RSRP from the reference signal in the preamble, the packet sequence number from the header, and the PER from the cyclic redundancy check (CRC). During handover, the source and target gNBs transmit identical packets. Wall-Street combines the downlink channels, enabling the UE to decode packets on both channels simultaneously and compute the combined PER. A C++ script in SB1 sends control commands to the gNB and Wall-Street to follow the procedure, as illustrated in Fig. 10 (right).

5 Evaluation

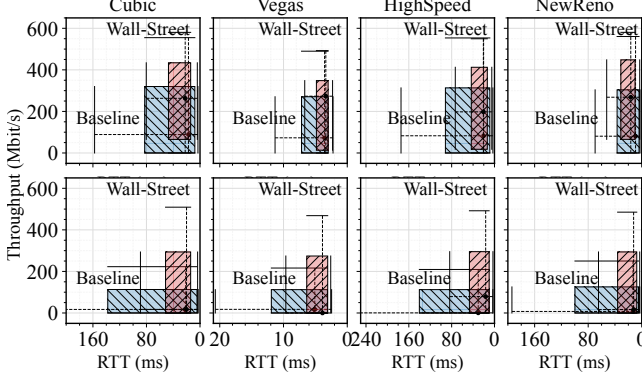
We first conduct field studies to evaluate the end-to-end performance of Wall-Street and compare it with a 3GPP standardized 5G SA handover protocol (§5.2). We then present micro-benchmark experiments to provide further insight into which factors impact Wall-Street’s performance (§5.3).

5.1 Methodology

We conduct evaluations of various indoor (single-UE) and outdoor (multi-UE) driving scenarios. For indoor settings, there are four gNB nodes and one UE node in a lab measuring 20×30 m, as shown in Fig. 11(b). To test the UE and Wall-Street under mobility, we place them on a cart moving in a constant speed of approximately 1 km/h. For outdoor settings, there are three gNB nodes on the first floor of a lab facing a parking lot. We mount the surface on the rear window of a SUV vehicle and deploy two UE nodes: UE 1



(a) Indoor TCP performance with one user.



(b) Outdoor TCP performance with two users (*upper*: UE 1; *lower*: UE 2).

Figure 13— Throughput and round trip time (RTT) achieved by four congestion control algorithms. The right and lower edge of the box represents the 10% percentile, respectively. The left and upper edge give the 90% percentiles. The intersection point of the horizontal and vertical error bar represents the median value.

on the opposite side of the rear seat and UE 2 on the trunk, as shown in Fig. 11(c). Both UEs face the rear window. The vehicle travels at speeds ranging from 5 to 15 km/h. Both the surface and UEs are battery-powered, with UE positions remaining constant for the baseline tests. Since stationary PAAMs cannot be moved, our outdoor trajectory is limited to 30 m, as depicted in Fig. 12.

We implement the 5G SA HO protocol described in §2 and deploy it on our testbed for comparison. We term this scheme as the baseline, using it as a performance benchmark in the remainder of our evaluation. For both Wall-Street and baseline, the hysteresis parameter H of A3 event in Eq. (1) is set to 10 dB with TTT of 150 ms and the measurement report periodicity of 160 ms. For the baseline, a total duration of every measurement report takes less than 20 ms with three neighbor gNBs. We set our time-to-handover to 300 ms. The outdoor testbed yielded a maximum RSRP of about 10 dB. In the ns-3 simulator, we increased all outdoor RSRP traces by 10 dB for both the baseline and Wall-Street scenarios.

5.2 End-to-end Throughput and Delay

We evaluate end-to-end performance of Wall-Street delivering bulk TCP data flows. To quantify performance, we

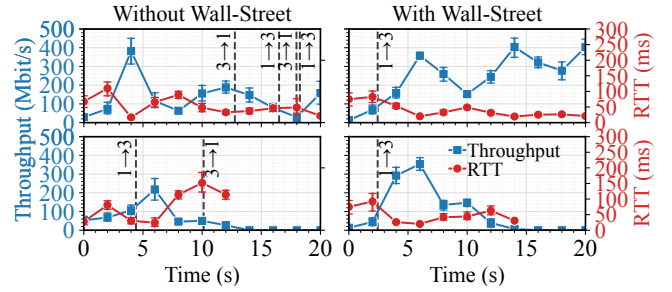


Figure 14— Throughput and delay of UE 1 (*upper*) and UE 2 (*lower*) achieved without Wall-Street (*left*) and with Wall-Street (*right*) as the vehicle is moving along the same trajectory. Vertical dashed lines indicate the handover event.

calculate throughput as the total data bits divided by the duration, measured every 100 ms. We average the round-trip-time (RTT) of packets over every 100 ms.

TCP performance under various settings. We evaluate the throughput and RTT of Wall-Street and the baseline under indoor and outdoor settings using four congestion control algorithms: CUBIC, Vegas, HighSpeed, and NewReno. In the indoor setting (Fig. 13(a)), Wall-Street enhances average throughput by at least 20% and reduces delay by 20-80% compared to the baseline. For the outdoor multi-user scenario (Fig. 13(b)), Wall-Street yields even more significant improvements: for UE 1 (*upper*), it doubles the average throughput and reduces RTT by 16%, while for UE 2 (*lower*), it increases throughput by 90% and decreases RTT by 45% on average. Notably, in the baseline setup, UE 2 (located in the trunk) experiences lower throughput and higher RTT than UE 1. Wall-Street improves signal coverage for UE 2, mitigating these issues.

TCP performance over time. To further demonstrate Wall-Street's performance, we divide the outdoor multi-user experiment into 10 equal intervals of two seconds each. Fig. 14 shows the median throughput and delay for UE 1 (*upper*) and UE 2 (*lower*) in each interval, comparing Wall-Street to the baseline. Vertical dashed lines indicate handover events. Wall-Street consistently outperforms the baseline in throughput throughout the experiment while demonstrating lower latency and significantly fewer handover ping-pongs between gNB 1 and 3. Notably, with Wall-Street, both UEs undergo handover simultaneously at the 2s mark, streamlining the process compared to the baseline where UE 1 and UE 2 handed over at different times. Moreover, Wall-Street maintained a stable connection throughout, whereas the baseline experienced an outage for UE 1 at 18s, immediately following a handover. These results demonstrate Wall-Street's capacity to enhance throughput, reduce latency, optimize handovers, and improve connection stability. in multi-user scenarios.

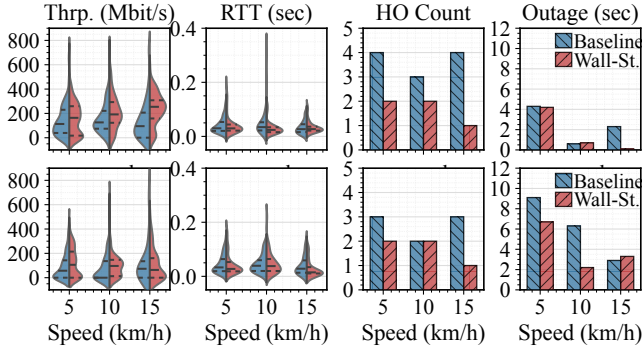


Figure 15— Impact of speed under the multi-user scenario: throughput, RTT, HO count, and total outage duration (left to right) with different speed, ranging from 5 km/h to 15 km/h (upper: UE 1; lower: UE 2).

Impact of vehicle speed. Figure 15 compares Wall-Street’s performance against the baseline for UE 1 (upper) and UE 2 (lower) at driving speeds from 5 km/h to 15 km/h. Wall-Street consistently outperforms the baseline across most metrics and speed scenarios. For UE 1, Wall-Street delivers throughput gains of 13%, 30%, and 61% at 5 km/h, 10 km/h, and 15 km/h respectively, while UE 2 sees gains of 34% and 21% for 5 km/h and 10 km/h. Also, Wall-Street reduces handover frequency by an average of 53% for UE 1 and 33% for UE 2, while also reducing outage duration by an average of 27% for UE 1 and 26% for UE 2. This shows Wall-Street’s robustness and ability to maintain stable performance under varying mobility conditions. Notably, UE 2 experiences longer outage durations due to its location in the trunk, where the car body easily obstructs the signal.

Impact of handover preparation. Figure 16 illustrates sequence number progression during the outdoor experiment, with the left subfigure showing the entire duration and the right subfigure focusing on the handover preparation phase. To enhance visibility of trends, sequence numbers are subjected to a modulo operation. Wall-Street allows a steeper increase in sequence numbers compared to the baseline, indicating that more packets are successfully delivered. During handover preparation, the baseline’s sequence numbers show irregular progression and a lower slope due to service interruptions as the UE stops communicating with the source gNB to detect SSB bursts from neighboring gNBs. While SSB detection takes under 20 ms, its effects persist for 50 ms, significantly disrupting baseline packet delivery. In contrast, Wall-Street maintains steady sequence number progression throughout the handover preparation phase, demonstrating more stable communication.

Impact of make-before-break handover. Figure 17 presents the cumulative distribution function (CDF) of the packet reception rate (PRR) during soft handover. PRRs are calculated

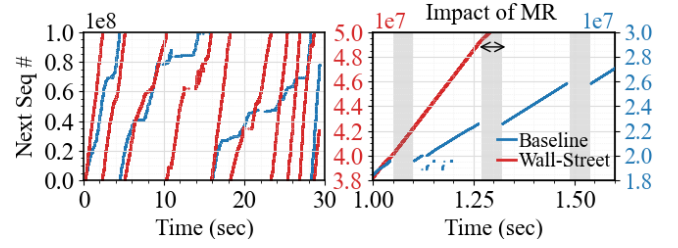


Figure 16— Measurement report impact: increase trend of sequence numbers during the entire 30s experiment (left) and handover preparation (right).

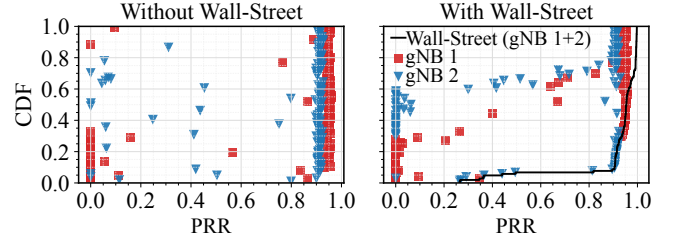


Figure 17— Make-before-break impact: packet reception rate of a link from each gNB without Wall-Street (left) and that of each gNB and of two links (packet duplication) from two gNB with Wall-Street along the same trajectory (right).

by decoding CRC for every 2000 packets and plotted on the same y-axis for both subplots. The black line represents Wall-Street’s combined PRR with packet duplication from gNB 1 and 2. In Fig. 17 (left), markers show PRRs for each link without Wall-Street, while Fig. 17 (right) shows PRRs for links through Wall-Street without packet duplication. Interestingly, individual links using Wall-Street exhibit lower PRRs compared to the baseline. This is because Wall-Street’s beam combining approach divides power across two links, resulting in weaker signal strength per link. However, by combining the beams and sending duplicate packets, Wall-Street ensures a PRR above 90% for 92% of handover execution times and eliminates instances of packet error. In contrast, the baseline system suffers from low PRR on each link, potentially leading to packet loss and performance degradation. These results suggest that Wall-Street’s make-before-break approach enhances handover reliability, particularly during moments of weak signal strength.

5.3 Microbenchmarks

We evaluate Wall-Street’s in-vehicle signal coverage, multi-beam operations at the physical layer, and far-field beam pattern measured with the spectrum analyzer.

In-vehicle mmWave coverage. To evaluate Wall-Street’s signal coverage enhancement, we conduct an experiment with the surface mounted on a vehicle’s rear window and a

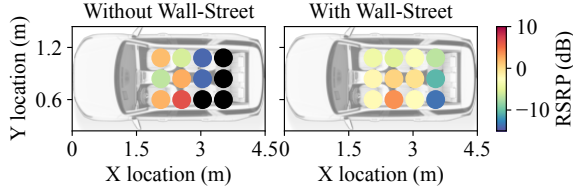


Figure 18— In-vehicle mmWave coverage. •: no signal.

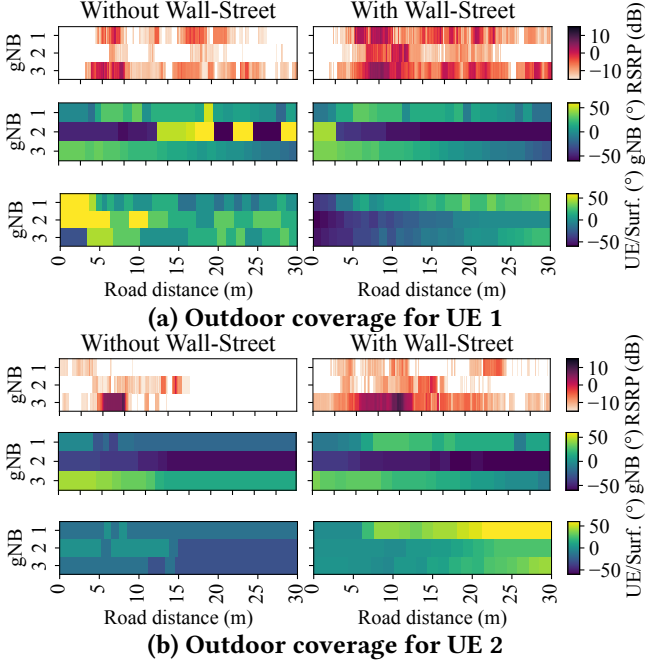
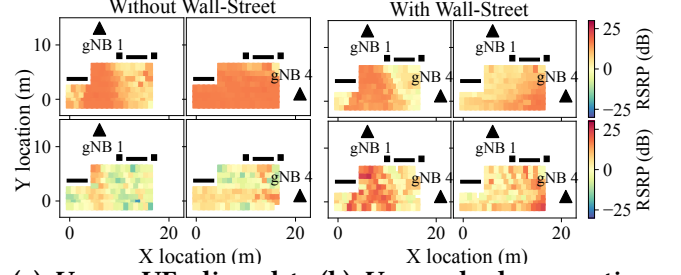


Figure 19— RSRP heatmap (*upper*) and corresponding gNB beam angles (*middle*) and UE/surface angles (*lower*) heatmaps (*left*: without Wall-Street; *right*: with Wall-Street and UE beam fixed to the surface). In-vehicle location of the UE is the same in both scenarios.

gNB positioned 30 meters away. We measure the maximum RSRP at various in-vehicle UE locations, exhaustively searching through combinations of gNB and UE beam angles and surface steering angles. For Wall-Street, the UE's receiving beam is fixed towards the surface. As illustrated in Fig. 18, Wall-Street significantly outperforms the baseline. While the baseline experiences signal outage for UEs in the backseat area, Wall-Street ensures outage-free coverage throughout the entire vehicle interior. Furthermore, Wall-Street provides a substantial signal strength improvement with over 12 dB gain at various in-vehicle locations.

Beam tracking under mobility. Figure 19 illustrates the RSRPs and corresponding beam angles for gNB and UE/surface as the vehicle traverses a 30-meter outdoor path, with separate plots for UE 1 (Fig. 19(a)) and UE 2 (Fig. 19(b)). In the Wall-Street setup, the UE angle is fixed towards the surface.



(a) *Upper*: UE aligned to the gNB; *lower*: UE not from two gNBs; *lower*: inferred MR. (b) *Upper*: dual connection the gNB; *lower*: UE not from two gNBs; *lower*: inferred MR.

Figure 20— RSRP heatmap without and with multi-link operations. gNB \blacktriangle , UE \square , blockage \blacksquare .

The gNB angle distributions remain similar for both Wall-Street and baseline scenarios. However, Wall-Street demonstrates better signal coverage overall. This improvement is particularly evident for UE 2, which loses all gNB signals beyond the 15-meter mark in the baseline setup, whereas Wall-Street maintains signal coverage from gNB 1 and/or 3 throughout the entire path.

Multi-link operations. We evaluate Wall-Street's capability to manipulate multiple beams at various indoor locations. Fig. 20 compares RSRP heatmaps with and without Wall-Street. Fig. 20(a) shows single-link baseline scenarios: upper heatmaps with UE beams aligned to gNB 1's beams (left) or gNB 4's beams (right), and lower heatmaps with gNB 1's beams (left) or gNB 2's beams (right) directed at the UE but UE angle fixed at 0° . Fig. 20(b) illustrates Wall-Street's multi-link scenarios: upper heatmaps during make-before-break handover execution, and lower heatmaps during handover preparation. The upper heatmaps in Fig. 20(b) show received RSRPs from gNB 1 (left) and gNB 4 (right) during the simultaneous packet reception. Due to power splitting, these RSRP values are slightly less than the aligned, single-link scenario. The lower heatmaps in Fig. 20(b) depict inferred RSRPs from packets received at gNB 1 (left) and gNB 4 (right) as Wall-Street reflects signals. These results demonstrate that signals reflected by Wall-Street can be accurately inferred, validating the method described in §3.3.1.

Far-field beam patterns. Figure 21 illustrates beam patterns for Wall-Street's four operation modes: beam split, single-directional beam combination, bi-directional beam combination, and bi-directional beam splitting. We select four beam angle sets ($-40^\circ/40^\circ$, $-40^\circ/55^\circ$, and $-68^\circ/45^\circ$) near the intersection of two gNBs' coverage areas, each with a 0.2 km radius. To measure beam patterns, we position transmit and receive horn antennas two meters from Wall-Street, recording its gain as we move the receiver from -70° to 70° .

Due to the absence of an anechoic chamber, beams passed around the surface. To ensure accurate pattern capture, we

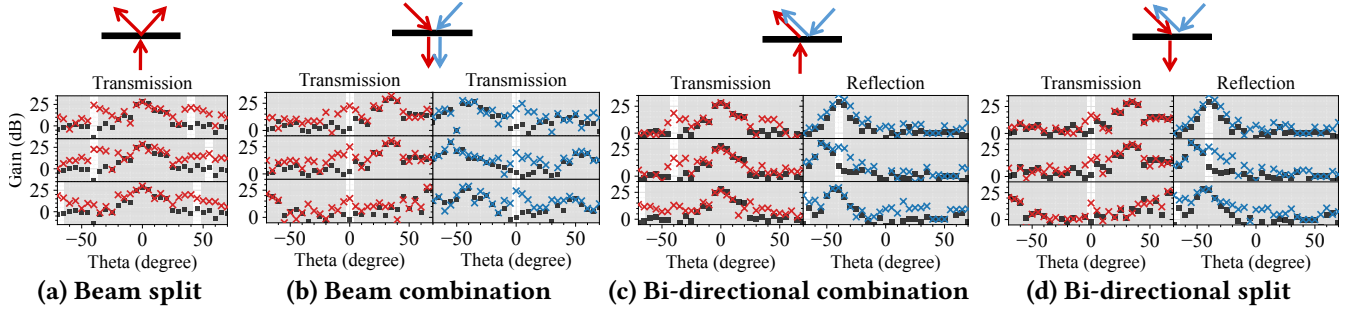


Figure 21— Wall-Street’s beam patterns over four operations. \times : empirical spectrum analyzer data; \blacksquare : benchmark data with the surface is set to 0V. The steering angles are highlighted in the background. 0 dB represents the spectrum analyzer noise floor (*upper*: $-40^\circ/40^\circ$; *middle*: $-40^\circ/55^\circ$; *lower*: $-68^\circ/45^\circ$). Red and blue markers are measured at 26 GHz and 26.1 GHz, respectively.

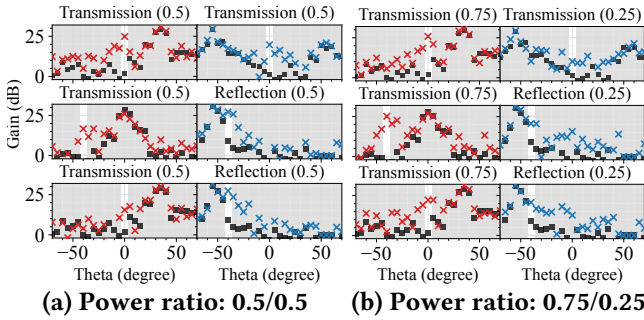


Figure 22— Power ratio adjustment with the steering angle of $-40^\circ/55^\circ$ (*upper*: beam combination; *middle*: bi-directional combination; *lower*: bi-directional split).

measure patterns with Wall-Street set to 0V (not steering the incident beam), using these as benchmarks (denoted by \blacksquare). We set 0 dB as the spectrum analyzer’s noise floor and scale results accordingly. Wall-Street operates on two channels: left transmitter (red arrows) at 26 GHz and right transmitter (blue arrows) at 26.1 GHz.

Compared to the benchmark, we observe 20-25 dB gain in each direction, except when a steered beam aligns with the transmitter’s specular reflection (e.g., $-40^\circ/40^\circ$ reflection in Fig. 21(c) and Fig. 21(d)). Wider beam steering angles result in decreased gain. Identical voltage configurations in Figs. 21(a) and 21(b) demonstrate that angular reciprocity holds even under multi-beam operation, enabling rapid uplink/downlink packet flow switching during handover.

Beam power ratio. Figure 22 compares beam patterns with different power ratios: 0.5/0.5 and 0.75/0.25 split. Across all three multi-beam operations, shifting the ratio from 0.5/0.5 to 0.75/0.25 results in increased gain for the left beam (red markers) and decreased gain for the right beam (blue markers). This demonstrates Wall-Street’s ability to flexibly adjust power distribution between two beams.

6 Related Work

Prior electronically-tunable mmWave and THz surface designs steer a single link at the physical layer using various techniques: relay switches and phase delay lines controlling patch antennas in a reflective configuration [27], PIN diodes controlling patch antennas in a reflective configuration [8, 9, 32], varactor diodes controlling patch antennas in a reflective configuration [30], or varactor diodes controlling split ring resonators in a Huygens reflective-transmissive configuration [6]. Other designs take an actively-amplified, amplify-and-forward approach at the physical layer [4]. Some THz designs are similar in concept yet differ in substrate, leveraging switched 65 nm CMOS process controlling ring resonators for a 0.3 THz design [29]. However, these proposals stop short of co-designing the surface’s involvement with 5G’s handover protocol and RAN architecture as Wall-Street does. NR-Surface [15] is a 24 GHz, varactor-controlled patch antenna reflective surface that integrates with 5G New Radio’s beam management, but does not offer a transmissive mode as Wall-Street does, for the common case where the client and cell are on opposite sides of the surface. Further, our experimental evaluation probes end-to-end, transport-layer performance, going beyond NR-Surface’s strictly physical-layer measurement results.

Prior passive/static mmWave reflector designs leverage electronic beam steering capabilities of base stations and clients with typically larger surfaces that reflect in many different directions. At 60 GHz, MilliMirror [22] proposes a novel, 3D-printed surface synthesis algorithm. However, similarly to prior electronically-tunable surface work, these systems also stop short of 5G RAN co-design.

Prior roadside/trackside handover designs Polycorn [21] and Wi-Fi Goes to Town [26] orchestrate packet flow for LTE and Wi-Fi trackside and roadside networks, respectively, transferring packets from one cell or access point in the radio access network in order to best serve highly-mobile users. Wall-Street, in contrast, leverages the unique capabilities

of smart surfaces and mmWave communications to split and combine beams to and from roadside mmWave cells in a way these prior designs do not anticipate. REM [16] uses Orthogonal Time Frequency Modulation in the LTE low band to simplify the conventional low-band signal strength based handover sequence, but does not target the larger frequency bandwidths and smaller cell sizes of mmWave 5G.

Work in mmWave beam alignment maintains a connection once it has been established via beam search. Representative works include Agile-Link [12], which proposes multi-armed beams and a postprocessing algorithm to accelerate the alignment time to be logarithmic in the number of possible beam directions. LiSteer [10] uses mmWave access point indicator LEDs and an array of mobile client-mounted light sensors to infer client bearing to the access point. BounceNet [14] proposes an architecture and algorithm for aligning many walking speed clients' 802.11ad links with many nearby 60 GHz access points, in a relatively dense access point deployment scenario, targeting a different problem than Wall-Street.

7 Conclusion

This paper introduces Wall-Street, the first smart surface-enabled 5G mmWave roadside networking solution designed to efficiently steer outdoor mmWave signals into vehicles, enable simultaneous data exchange and neighboring cell measurements, and facilitate seamless and reliable handovers through a make-before-break process. We conduct an extensive evaluation in various indoor and outdoor multi-user settings, demonstrating significant TCP improvement. We believe Wall-Street is the first step in scaling out the capacity of mmWave networks and paves the way for future advancements in mmWave communications, particularly in vehicular networks.

8 Acknowledgements

This material is based upon work supported by the National Science Foundation under Grants No. CNS-2148271 and CNS-2232459, and is supported in part by funds from federal agency and industry partners as specified in the Resilient & Intelligent NextG Systems (RINGS) program. We gratefully acknowledge the support of a grant from the Princeton University School of Engineering and Applied Science Innovation Fund.

References

- [1] 3GPP. 2017. *Study on new radio access technology physical layer aspects*. Technical Report (TR) 38.802. 3rd Generation Partnership Project (3GPP).
- [2] 3GPP. 2021. *5G; NR; NR and NG-RAN Overall description; Stage-2*. Technical Report (TR) 38.300. 3rd Generation Partnership Project (3GPP). https://www.etsi.org/deliver/etsi_ts/138300_138399/138300/16.04.00_60/ts_138300v160400p.pdf
- [3] 3GPP. 2022. *Release 17 Description; Summary of Rel-17 Work Items*. Technical Report (TR) 21.917. 3rd Generation Partnership Project (3GPP). <http://www.3gpp.org/DynaReport/21917.htm>
- [4] Omid Abari, Dinesh Bharadia, Austin Duffield, and Dina Katabi. 2017. Enabling High-Quality Untethered Virtual Reality. In *14th USENIX Symposium on Networked Systems Design and Implementation (NSDI)*. 531–544. <https://www.usenix.org/conference/nsdi17/technical-sessions/presentation/abari>
- [5] Yaniv Azar, George N. Wong, Kevin Wang, Rimma Mayzus, Jocelyn K. Schulz, Hang Zhao, Felix Gutierrez, DuckDong Hwang, and Theodore S. Rappaport. 2013. 28 GHz propagation measurements for outdoor cellular communications using steerable beam antennas in New York city. In *IEEE International Conference on Communications (ICC)*. 5143–5147. <https://doi.org/10.1109/ICC.2013.6653399> ISSN: 1938-1883.
- [6] Kun Woo Cho, Mohammad H. Mazaheri, Jeremy Gummeson, Omid Abari, and Kyle Jamieson. 2023. mmWall: A Steerable, Transflective Metamaterial Surface for NextG mmWave Networks. In *20th USENIX Symposium on Networked Systems Design and Implementation (NSDI)*. 1647–1665. <https://www.usenix.org/conference/nsdi23/presentation/cho-kun-woo>
- [7] Haotian Deng, Chunyi Peng, Ans Fida, Jiayi Meng, and Y. Charlie Hu. 2018. Mobility Support in Cellular Networks: A Measurement Study on Its Configurations and Implications. In *Proceedings of the Internet Measurement Conference 2018*. ACM, Boston MA USA, 147–160. <https://doi.org/10.1145/3278532.3278546>
- [8] Jean-Baptiste Gros, Vladislav Popov, Mikhail A. Odit, Vladimir Lenets, and Geoffroy Lerosey. 2021. A Reconfigurable Intelligent Surface at mmWave Based on a Binary Phase Tunable Metasurface. *IEEE Open Journal of the Communications Society* 2 (2021), 1055–1064. <https://doi.org/10.1109/OJCOMS.2021.3076271>
- [9] Jean-Baptiste Gros, Luca Santamaria, Vladislav Popov, Mikhail Odit, Vladimir Lenets, Khoandri Lleshi, Ayoub Toubal, and Youssef Nasser. 2023. Design of Reconfigurable Intelligent Surfaces at mmWave with Application to 5G/6G. In *2023 17th European Conference on Antennas and Propagation (EuCAP)*. IEEE, Florence, Italy, 1–4. <https://doi.org/10.23919/EuCAP57121.2023.10133769>
- [10] Muhammad Kumail Haider, Yasaman Ghasempour, Dimitrios Koutsoukolas, and Edward W. Knightly. 2018. LiSteer: mmWave Beam Acquisition and Steering by Tracking Indicator LEDs on Wireless APs. In *Proceedings of the 24th Annual International Conference on Mobile Computing and Networking (MobiCom)*. ACM, New Delhi India, 273–288. <https://doi.org/10.1145/3241539.3241542>
- [11] Ahmad Hassan, Arvind Narayanan, Anlan Zhang, Wei Ye, Ruiyang Zhu, Shuwei Jin, Jason Carpenter, Z. Morley Mao, Feng Qian, and Zhi-Li Zhang. 2022. Vivisecting mobility management in 5G cellular networks. In *Proceedings of the ACM SIGCOMM 2022 Conference (SIGCOMM '22)*. Association for Computing Machinery, New York, NY, USA, 86–100. <https://doi.org/10.1145/3544216.3544217>
- [12] Haitham Hassanieh, Omid Abari, Michael Rodriguez, Mohammed Abdelghany, Dina Katabi, and Piotr Indyk. 2018. Fast millimeter wave beam alignment. In *Proceedings of the Conference of the ACM Special Interest Group on Data Communication (SIGCOMM)*. ACM, Budapest Hungary, 432–445. <https://doi.org/10.1145/3230543.3230581>
- [13] Ibrahim A. Hemadeh, Katla Satyanarayana, Mohammed El-Hajjar, and Lajos Hanzo. 2018. Millimeter-Wave Communications: Physical Channel Models, Design Considerations, Antenna Constructions, and Link-Budget. *IEEE Communications Surveys & Tutorials* 20, 2 (2018), 870–913. <https://doi.org/10.1109/COMST.2017.2783541>
- [14] Suraj Jog, Jiaming Wang, Junfeng Guan, Thomas Moon, Haitham Hassanieh, and Romit Roy Choudhury. 2019. Many-to-Many Beam Alignment in Millimeter Wave Networks. In *USENIX Symposium on Networked Systems Design and Implementation (NSDI)*. <https://www.usenix.org/conference/nsdi19/presentation/jog>
- [15] Minseok Kim, Namjo Ahn, and Song Min Kim. 2024. NR-Surface: NextG-ready μ W-reconfigurable mmWave Metasurface. In *USENIX Symposium on Networked Systems Design and Implementation (NSDI)*.
- [16] Yuanjie Li, Qianru Li, Zhehui Zhang, Ghufan Baig, Lili Qiu, and Songwu Lu. 2020. Beyond 5G: Reliable Extreme Mobility Management. In *Proceedings of the Annual conference of the ACM Special Interest Group on Data Communication on the applications, technologies, architectures, and protocols for computer communication*. ACM, Virtual Event USA, 344–358. <https://doi.org/10.1145/3387514.3405873>
- [17] George R. MacCartney, Theodore S. Rappaport, and Sundee Rangan. 2017. Rapid Fading Due to Human Blockage in Pedestrian Crowds at 5G Millimeter-Wave Frequencies. In *IEEE Global Communications Conference (GLOBECOM)*. IEEE, Singapore, 1–7. <https://doi.org/10.1109/GLOCOM.2017.8254900>
- [18] Marco Mezzavilla, Menglei Zhang, Michele Polese, Russell Ford, Sourjya Dutta, Sundee Rangan, and Michele Zorzi. 2018. End-to-End Simulation of 5G mmWave Networks. *IEEE Communications Surveys & Tutorials* 20, 3 (2018), 2237–2263. <https://doi.org/10.1109/COMST.2018.2828880>
- [19] Arvind Narayanan, Eman Ramadan, Jason Carpenter, Qingxu Liu, Yu Liu, Feng Qian, and Zhi-Li Zhang. 2020. A First Look at Commercial 5G Performance on Smartphones. In *Proceedings of The Web Conference (WWW)*. ACM, Taipei Taiwan, 894–905. <https://doi.org/10.1145/3366423.3380169>
- [20] Arvind Narayanan, Xumiao Zhang, Ruiyang Zhu, Ahmad Hassan, Shuwei Jin, Xiao Zhu, Xiaoxuan Zhang, Denis Rybkin, Zhengxuan Yang, Zhuoqing Morley Mao, Feng Qian, and Zhi-Li Zhang. 2021. A variegated look at 5G in the wild: performance, power, and QoE implications. In *Proceedings of the Conference of the ACM Special Interest Group on Data Communication (SIGCOMM)*. ACM, New York, NY, USA, 610–625. <https://doi.org/10.1145/3452296.3472923>
- [21] Yunzhe Ni, Feng Qian, Taide Liu, Yihua Cheng, Zhiyao Ma, Jing Wang, Zhongfeng Wang, Gang Huang, Xuanzhe Liu, and Chenren Xu. 2023. POLYCORN: Data-driven Cross-layer Multipath Networking for High-speed Railway through Composable Schedulerlets. In *20th USENIX Symposium on Networked Systems Design and Implementation (USENIX NSDI)*. 1325–1340.
- [22] Kun Qian, Lulu Yao, Xinyu Zhang, and Tse Nga Ng. 2022. MilliMirror: 3D printed reflecting surface for millimeter-wave coverage expansion. In *Proceedings of the 28th Annual International Conference on Mobile Computing And Networking (MobiCom)*. ACM, Sydney NSW Australia, 15–28. <https://doi.org/10.1145/3495243.3517024>
- [23] Sundee Rangan, Theodore S. Rappaport, and Elza Erkip. 2014. Millimeter-Wave Cellular Wireless Networks: Potentials and Challenges. *Proc. IEEE* 102, 3 (March 2014), 366–385. <https://doi.org/10.1109/JPROC.2014.2299397>
- [24] Theodore S. Rappaport, George R. MacCartney, Shu Sun, Hangsong Yan, and Sijia Deng. 2017. Small-Scale, Local Area, and Transitional Millimeter Wave Propagation for 5G Communications. *IEEE Transactions on Antennas and Propagation* 65, 12 (Dec. 2017), 6474–6490. <https://doi.org/10.1109/TAP.2017.2734159>

- [25] Dipankar Raychaudhuri, Ivan Seskar, Gil Zussman, Thanasis Korakis, Dan Kilper, Tingjun Chen, Jakub Kolodziejski, Michael Sherman, Zoran Kostic, Xiaoxiong Gu, Harish Krishnaswamy, Sumit Maheshwari, Panagiotis Skrimponis, and Craig Gutterman. 2020. Challenge: COSMOS: A city-scale programmable testbed for experimentation with advanced wireless. In *Proceedings of the 26th Annual International Conference on Mobile Computing and Networking (MobiCom '20)*. Association for Computing Machinery, New York, NY, USA, 1–13. <https://doi.org/10.1145/3372224.3380891>
- [26] Zhenyu Song, Longfei Shangguan, and Kyle Jamieson. 2017. Wi-Fi Goes to Town: Rapid Picocell Switching for Wireless Transit Networks. In *Proceedings of the Conference of the ACM Special Interest Group on Data Communication (SIGCOMM)*. ACM, New York, NY, USA, 322–334. <https://doi.org/10.1145/3098822.3098846>
- [27] Xin Tan, Zhi Sun, Dimitrios Koutsonikolas, and Josep M. Jornet. 2018. Enabling Indoor Mobile Millimeter-wave Networks Based on Smart Reflect-arrays. In *IEEE Conference on Computer Communications (INFOCOM)*. IEEE, Honolulu, HI, 270–278. <https://doi.org/10.1109/INFOCOM.2018.8485924>
- [28] Andrea Tassi, Malcolm Egan, Robert J. Piechocki, and Andrew Nix. 2017. Modeling and Design of Millimeter-Wave Networks for Highway Vehicular Communication. *IEEE Transactions on Vehicular Technology* 66, 12 (Dec. 2017), 10676–10691. <https://doi.org/10.1109/TVT.2017.2734684>
- [29] Suresh Venkatesh, Xuyang Lu, Hooman Saeidi, and Kaushik Sengupta. 2020. A high-speed programmable and scalable terahertz holographic metasurface based on tiled CMOS chips. *Nature Electronics* 3, 12 (Dec. 2020), 785–793. <https://doi.org/10.1038/s41928-020-00497-2>
- [30] Alexander Wolff, Lars Franke, Steffen Klingel, Janis Krieger, Lukas Mueller, Ralf Stemler, and Marco Rahm. 2023. Continuous beam steering with a varactor-based reconfigurable intelligent surface in the Ka-band at 31 GHz. *Journal of Applied Physics* 134, 11 (Sept. 2023), 114502. <https://doi.org/10.1063/5.0168330>
- [31] Dongzhu Xu, Anfu Zhou, Xinyu Zhang, Guixian Wang, Xi Liu, Congkai An, Yiming Shi, Liang Liu, and Huadong Ma. 2020. Understanding Operational 5G: A First Measurement Study on Its Coverage, Performance and Energy Consumption. In *Proceedings of the Conference of the ACM Special Interest Group on Data Communication (SIGCOMM)*. ACM, New York, NY, USA, 479–494. <https://doi.org/10.1145/3387514.3405882>
- [32] Fei Yang, Fan Xu, Chenxi Liu, Xinyu Yang, Ziqiang Wang, Junwei Wu, and Xiaojian Fu. 2022. Two-Dimensional Beam Steering Based on Compact Programmable Coding Metasurface. *Applied Sciences* 12, 22 (Jan. 2022), 11780. <https://doi.org/10.3390/app122211780>
- [33] Hang Zhao, Rimma Mayzus, Shu Sun, Mathew Samimi, Jocelyn K. Schulz, Yaniv Azar, Kevin Wang, George N. Wong, Felix Gutierrez, and Theodore S. Rappaport. 2013. 28 GHz millimeter wave cellular communication measurements for reflection and penetration loss in and around buildings in New York city. In *IEEE International Conference on Communications (ICC)*. 5163–5167. <https://doi.org/10.1109/ICC.2013.6655403> ISSN: 1938-1883.

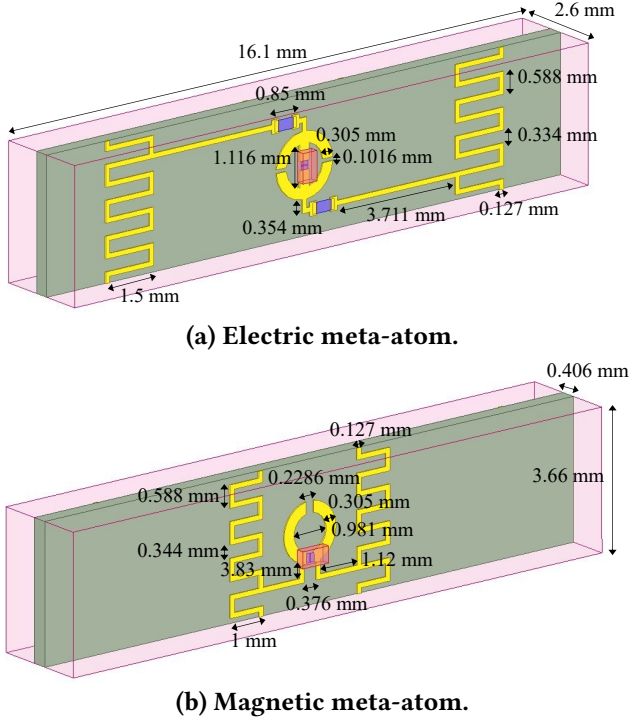


Figure 23— Wall-Street’s unit cell design parameters. The pink box is an air box that defines the boundary conditions to simulate the unit cell.

A Surface Design Parameters

In this section, we provide design parameters of Wall-Street’s electric and magnetic meta-atom, as illustrated in Fig. 23. The thickness of PCB Roger 4003C substrate is 0.406 mm and the thickness of the copper trace is 1 oz. To simulate the unit cell response, we create an air box that defines the boundary conditions. The top and bottom boundaries of the box are perfect electric boundary, and the front and back of the box are perfect magnetic boundary. We will publicly release all PCB design schematics, simulation scripts (HFSS and SPICE), and control codes.

B RSRP inference for HO decision.

The RSRP of the neighbor gNB’s measurement report as received by the source gNB, M_r , is distinct from M_n in Eq. (1), and so to apply Eq. (1), we need to derive a sound measurement for M_n based on the novel reflective measurement M_r that Wall-Street makes. As illustrated in Fig. 24, M_n is the signal strength between the neighboring gNB to UE through the surface (red dotted line). To infer M_n , Wall-Street uses the RSRP of a link between the source gNB and UE (M_s) and between the neighboring cell and the source gNB (M_r). We can simplify the link budget of each RSRP measurement as

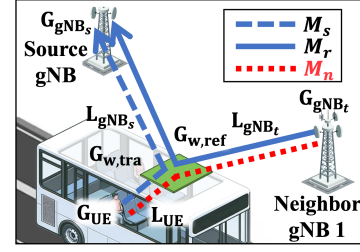


Figure 24— Measurement power translation: Inferring 3GPP-standard measurement report power readings based on Wall-Street’s reflective measurement report readings.

follows:

$$M_s = G_{gNB_s} + L_{gNB_s} + G_{w,tra} + G_{UE} + L_{UE} + L_{car} \quad (2)$$

$$M_n = G_{gNB_n} + L_{gNB_n} + G_{w,tra} + G_{UE} + L_{UE} + L_{car} \quad (3)$$

where G_{gNB_s} and G_{gNB_n} are the gain of the source and neighbor gNBs respectively, L_{gNB_s} and L_{gNB_n} are the free-space path loss between the source and neighbor gNBs and the surface, respectively, $G_{w,tra}$ is the transmission gain of the surface, G_{UE} is the gain of the UE, L_{UE} is the free-space path loss between the UE and the surface, and L_{car} is the loss from a car window. Likewise, we can calculate the signal strength measured by the source gNB (M_r) as:

$$M_r = G_{gNB_n} + L_{gNB_n} + G_{w,ref} + G_{gNB_s} + L_{gNB_s} + 2 \cdot L_{car} \quad (4)$$

where $G_{w,ref}$ is the reflection gain of the surface. Summing Eqs. (2) and (3), we calculate M_n as

$$M_n = M_r - M_s - G_{w,ref} + 2 \cdot (G_{w,tra} + G_{UE} + L_{UE}). \quad (5)$$

We assume the UE-to-surface distance d_{UE} as the maximum possible distance between Wall-Street and the in-vehicle UE. This assumption is based on the fact that signals passing through the surface should reach all corners of the vehicle, particularly since all other UEs in the same vehicle are handed over simultaneously. We then calculate the path loss L_{UE} as $(4\pi d_{UE}/\lambda)^2$ where λ is a wavelength.

Since the source gNB controls the reflecting surface, it has knowledge of the surface’s reflective gain $G_{w,ref}$ and transmissive gain $G_{w,tra}$. Also, as the gNB controls the transmit power of the UE in 3GPP,² it also knows the UE’s transmit gain G_{UE} . By utilizing this information, the source gNB can infer the RSRP between the target cell and the UE, enabling it to make effective handover decisions.

²The gNB sends Downlink Control Information (DCI) to send power control commands to the UE.